Computational Model and Flow Analysis in a Complex Manifold Configuration Under Steady State Turbulent Flow Conditions

Edoardo Gambacorta | 22231205 | *ucemeg3@ucl.ac.uk*

***Abstract*— The following study examines flow analysis in a complex manifold configuration and its properties. The intake manifold is an important component used in automotives to distribute air uniformly through to the engine cylinders, playing a major role in an engine's performance. The problem was redefined into a simple 2D geometry, consisting of one inlet and three outlets. Simulations were conducted using Computational Fluid Dynamics software CFD-ACE+, which is based on the Finite Volume Method (FVM). Both laminar and turbulent cases were explored, with Reynold's numbers ranging from 1^2 to 1^5. A mesh dependency study was completed in both cases, to ensure grid independency was achieved. Flow features were examined in laminar and turbulent regimes, and more defined vortices or backflow were identified at higher velocities. Pressure drops were analyzed at the three outlets by examining static pressure at increasing Reynold's numbers. Results were in accordance with the Hagen-Poiseuille equation, which suggests a linear relationship between pressure and flow velocity. Lastly, intake uniformity was assessed at different velocities, with similar results for each case. The base geometry exhibited poor distribution between the three outlets. Three new geometries were iterated to promote uniformity, and a final improved design was suggested.**

INTRODUCTION

The intake manifold, better known as inlet manifold, is used in automotive engineering to distribute air into the engine cylinder, which is used in the combustion process. It also plays a role in the cooling of cylinders, which prevents the engine from overheating [1]. Manifolds are equipped with a fuel injector, which dispenses the fuel into the engine efficiently [2]. In older cars, (without a fuel injector) the manifold directly delivers the fuel-air mixture from throttle body to the cylinder heads. For an engine to perform optimally, there must be an even distribution of the gas at the manifold outlets.

Typically, inlet manifolds are fabricated from aluminum or cast iron, yet it is not uncommon for cars to use plastic manifolds. The design of the intake manifold can vary depending on the desired application. Major considerations include shape, length, and section area. An inlet manifold's primary function is to provide a stable air intake for the engine, ensuring equal dispersion or uniformity in each cylinder [3]. This is crucial for an engine's performance, as a poorly functioning manifold can affect emissions, engine vibrations and torque output. Thus, developing the intake manifold is a critical technology in assuring engine power, economy, dependability, and emission quality [3].

Inlet manifold performance is dependent on the following design criteria. To begin, altering the air inlet direction, regulator chamber volume, and manifold outlet direction can improve gas liquidity and flow quality [3]. Another important aspect is for the intake manifold to exhibit a supercharging effect. For this to occur, all the geometric parameters of the intake manifold must be aligned. This sequence of synchronized events is referred to as 'resonant conditions' [4]. Factors that impact resonance charging include: the length of manifold outlets and the manifold cavity volume. When these are optimized, it will improve the dispersion of intake air into the cylinders. Lastly, by interpreting the mass flow rate equation, it can be inferred that the manifold inlet length is correlated to the air mass flow rate into the manifold, which is determined by its respective diameter. Similarly, volume flow rate equation suggests that manifold outlets impact the volume of gas flowing into the cylinders, so also involves its diameter.

Conducting a flow analysis for a certain inlet manifold geometry can prove highly beneficial in assessing its efficiency before it is tested in an engine. Computational fluid dynamics, or CFD is a branch of fluid mechanics that analyses, simulates, and solves fluid flow issues using numerical analysis and data structures. As computers continue to evolve and advance, CFD simulations have not only become easier to operate, but also more accurate and affordable. Analysis in this project was conducted using ESI Group's ACE+ CFD package, which is programmed around the fundamental principles of the Finite Element Method.

A 2D geometry of an inlet manifold has been provided, (refer to figure 1). The geometry in figure 1 includes one flow inlet with a 50mm diameter, and three 40mm diameter outlets at 90 degrees to the regulator chamber, with an area of 220x80mm. The following dimensions will be utilized to conduct the CFD simulations. In the beginning stage, the 2D geometry was created using CFD-view, part of the ACE+ suite package, where one is able to sketch and mesh geometries. The following configuration was simulated at a laminar case, with an inlet velocity of 0.1m/s. To examine the turbulence under steady-state conditions, various inlet velocities were simulated in the intake manifold. Turbulent flows were simulated at 5 inlet velocities of 2m/s, 5m/s, 10m/s, 20m/s, 28m/s. These all respectively have a Reynold's number above 3500, which justifies the flow is indeed turbulent. An unstructured mesh was used in the following simulations, ranging from roughly 30k to 480k elements. The benefit of utilizing an unstructured mesh in this investigation is it possesses the ability to conform to nearly any geometry [5]. While unstructured geometries have good precision and reasonably fast convergence, it is crucial to note that they have higher memory requirements and may take longer to solve [5]. In this investigation, the k-ε turbulence model was used, implementing standard wall functions. A mesh dependency study was conducted in both a laminar and turbulent case.

Investigating flow analysis in complex manifold configurations provides useful insights to understand its performance under steady-state turbulent conditions. Other objectives for this project include investigating how flow features change at higher Reynolds number, how the pressure drops vary from inlet to outlet at different Reynold's number, comparing back to laminar flow, and evaluating the intake uniformity by inspecting mass flow rates at each outlet. Different geometries were formulated and tested under the same velocities and solver conditions, which allowed for an accurate comparison and an understanding of the parameters that affect intake manifold performance. In this investigation, 3 different configurations were designed and compared against the base case geometry, shown in Figure 1. The improved geometries are discussed and analyzed at the end of the report.

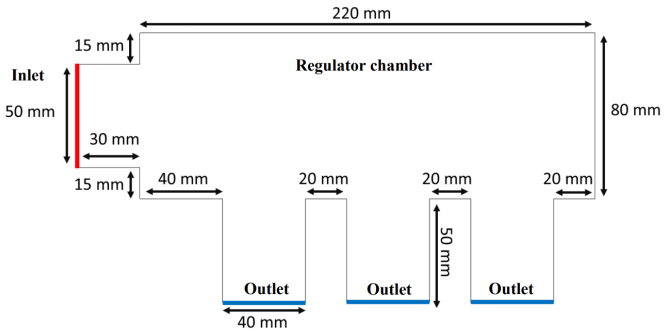

Figure 1: 2D geometry of the Manifold

METHODOLOGY

The CFD-ACE+ package offers an interesting variety of modules, including spraying, plasma, micro particles etc. In this study, only flow and turbulence module will be used. An advantage of the software is that it allows modelling of virtually any gas or liquid, through manipulating density and dynamic viscosity values in the Volume Conditions (VC) tab. All CFD simulations in this software were conducted using the Finite Volume Method (FVM). FVM is the most widely used and well-established numerical method in CFD for its clear relationship between the numerical algorithms and the physical conservation principles behind it [6].

The numerical algorithm can be described by the following process: [6]

- Integration of governing equations, determining fluid flow throughout all the domain's (finite) control volumes (cells)
- In the discretization step, the resulting integral equations are converted into a set of algebraic equations.
- Finally, an iterative approach is used to solve the algebraic equations.

To begin, CFD-ACE+ Geom was used to sketch a 2D inlet manifold geometry and define inlet, walls, and outlets, providing dimensions in mm (refer to Figure 1).

Mathematical Governing Equations

CFD-ACE+ uses Navier-Stokes equation flow as its primary solver. Flow module governing equations are based on the following statements: fluid mass is conserved, meaning the system does not lose or gain mass, and the rate of change of momentum is equated to the sum of forces of fluid, following Newton's second law of motion. Thus, only mass conservation and momentum conservation equations are used in the flow module, considering no heat transfer is present in this problem. The turbulent case is defined by 2D steady flow models. The k- ε model was also used in the model setup, for its robustness and ability to adapt to a range

of scenarios. Wall functions, or boundary layers have also been implemented in this model to link the inner region between the walls and the fully established turbulence region [7]. This allows for a significant reduction in the mesh size and therefore computational power required.

Mass Conservation Equations

The conservation of mass principle states that the rate of change of mass, in a control volume system is balanced by the net mass flow into the same control volume. This means inflow in a system is equal to the outflow. Mathematically, it can be expressed by: [8]

$$\frac{\partial \rho}{\partial t} + \nabla * \overrightarrow{(\rho V)} = 0$$

Where $\frac{\partial \rho}{\partial t}$ denotes the rate of change of mass-density (mass per unit volume and $\nabla * \overrightarrow{(\rho V)}$ is the convective term establishing the net mass flow across the control volume's boundaries.

Momentum Conservation Equations

The CFD-ACE+ software makes use of the x-component of the momentum equation. Similarly, this can be expressed as y-component as well as the z-component. These can be expressed as follows: [8]

x-component

$$\frac{\partial(\rho u)}{\partial t} + \nabla * \overrightarrow{(\rho u V)} = -\frac{\partial p}{\partial x} + \frac{\partial \tau_{xx}}{\partial x} + \frac{\partial \tau_{yx}}{\partial y} + \frac{\partial \tau_{zx}}{\partial z} + p f_x$$

y-component:

$$\frac{\partial(\rho v)}{\partial t} + \nabla * \overrightarrow{(\rho v V)} = -\frac{\partial p}{\partial y} + \frac{\partial \tau_{xy}}{\partial x} + \frac{\partial \tau_{yy}}{\partial y} + \frac{\partial \tau_{zy}}{\partial z} + p f_y$$

z-component:

$$\frac{\partial(\rho w)}{\partial t} + \nabla * \overrightarrow{(\rho w V)} = -\frac{\partial p}{\partial z} + \frac{\partial \tau_{zx}}{\partial x} + \frac{\partial \tau_{yz}}{\partial y} + \frac{\partial \tau_{zz}}{\partial z} + p f_z$$

Where τ represents shear stress, p is pressure and S_{M_i} is the momentum source term. Together, these equations can be described as Navier-Stokes equations in conservation form, and represent the governing equations used in the CFD-ACE+ solver.

Standard k-ε turbulent model

When inspecting flows in the laminar regime, one can refer to the mass conservation and momentum conservation equations described above. However, upon reaching Reynold's number values that are considered turbulent, it leads to a radical change in flow character, through random and chaotic behavior. A turbulent flow can be described by irregular flows characterized by eddies, swirls, and flow instabilities, driven by high momentum convection and low momentum diffusion [9].

To overcome this, the standard k-ε model is applied to the simulation. The k-ε model focuses on the mechanisms affecting turbulent kinetic energy and is one of the most widely used and accepted models to describe turbulent flows. At its core, this model uses two transport equations; the turbulent kinetic energy and its dissipation rate, which are represented by the following equations: [6]

Turbulent kinetic energy, k

$$\frac{\partial(pk)}{\partial t} + div(pk\boldsymbol{U}) = div\left[\frac{\mu_t}{\sigma_k} grad\ k\right] + 2\mu_t S_{ij} \cdot S_{ij} - \rho\varepsilon$$

Dissipation rate, ε

$$\frac{\partial(p\varepsilon)}{\partial t} + div(p\varepsilon\boldsymbol{U}) = div\left[\frac{\mu_t}{\sigma_\varepsilon} grad\ \varepsilon\right] + C_{1\varepsilon} 2\mu_t S_{ij} \cdot S_{ij} - C_{2\varepsilon}\rho\frac{\varepsilon^2}{k}$$

Turbulent viscosity, μ_t

$$\mu_t = \rho C_\mu \frac{k^2}{\varepsilon}$$

Where the five constants used are [6]:
$C_\mu = 0.09$, $C_{\varepsilon_1} = 1.44$, $C_{\varepsilon_2} = 1.92$, $\sigma_k = 1.0$, $\sigma_\varepsilon = 1.3$

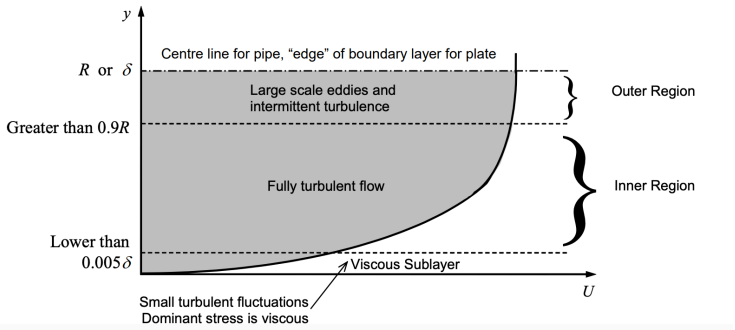

Fig.2 Near wall region in complex turbulent flows [32]

The standard k-ε turbulence model operates at high Reynold's numbers, so it is not appropriate for the near wall regions of the geometry, where viscous effects dominate the effects of turbulence. Specifically, the viscous sub layer, which is thin and requires many grid points to be resolved (see Figure 2). To overcome this issue, wall functions are applied in the near wall cell region, where wall parallel velocity can be obtained from: [10]

$$u^+ = y^+ \quad and \quad u^+ \leq y_v^+$$
$$u^+ = \frac{1}{k}\ln(Ey^+) \ where\ y^+ > y_v^+$$

$$y^+ = y\frac{u_\tau}{v} \quad and \quad u^+ = y\frac{u}{u_\tau}$$

$$u_\tau = C_\mu^{1/4} k^{1/2}, \quad k = 0.4, E = 9.0 \; for \; smooth \; walls$$

Grid generation, boundary conditions and initial set up

To carry out an accurate simulation, appropriate set up conditions must be specified in the ACE+ software. In this case, intake manifolds primarily focus on the dispersion of air, so a density of 1.225 kg/m^3, dynamic viscosity of 1.789 m^2/s and a reference pressure of 100,000 Pa have been accounted for.

This project is firstly carried out at laminar flow with a horizontal velocity of 0.1 m/s. However, the intake manifold has "air-fuel mixture flowing through at a maximum velocity of up to 167m/s" which is considered a turbulent flow [11]. Thus, in this investigation one must consider turbulent flows, which mainly involves Reynold's numbers, and is defined through the ratio of fluid momentum force to viscous shear force [12]. If the Reynold's number is less than 2000, the flow can be considered laminar. Flows between 2000 and 3500 are classified as transitional, whereas flows above 3500 are considered turbulent [13]. Through the Reynold's number, it is possible to assess the relevant velocities to carry out, which have chosen to be 0.1, 2, 5, 10, 20 and 28 m/s respectively.

Velocity (m/s)	Reynold's Number
0.1	342.4
2	6847
5	17119
10	34237
20	68474
28	95864

Figure 3 Flow velocities and their respective Reynold's numbers

Solving for Reynold's number will also allow to appropriately assess Turbulent Kinetic Energy and Dissipation Rate. These were computed in the simulation with the following equations: [10]

$$k = \frac{3}{2}(IU^2) \; where \; I = 0.16Re^{1/8}$$

$$\varepsilon = C_\mu \frac{k^{3/2}}{l}$$

$$where \; U \; is \; velocity \left(\frac{m}{s}\right), Re \; is \; Reynold's \; number$$

$$and \; l = 0.03L, (L \; is \; diameter \; of \; inlet \; in \; meters)$$

Central differencing was configured in the set-up, ensuring more accurate results compared to first order upwind scheme. However, this spatial differencing scheme can encounter issues in converging. Thus, a blending factor of 0.6 was used between the two, to verify that the solution converges and is more accurate than the typical first-order Upwind Differencing Scheme [10].

Before running the simulations, unstructured triangular grid meshes were constructed, ranging from 1k-500k elements. In the laminar case, a simple unstructured grid was sufficient, but since this investigation mainly involves turbulent flows, boundary layer meshing was applied in subsequent simulations. A clear advantage of this approach is its use of flow physics to set normal mesh spacings near the walls, instead of using less effective error indicators [14]. It also helps resolve the previously discussed issue of operating the k-ε turbulence model at near wall regions (see Figure 2). The final chosen mesh, and detailing on the boundary layers applied, can be viewed in Figures 4 & 5.

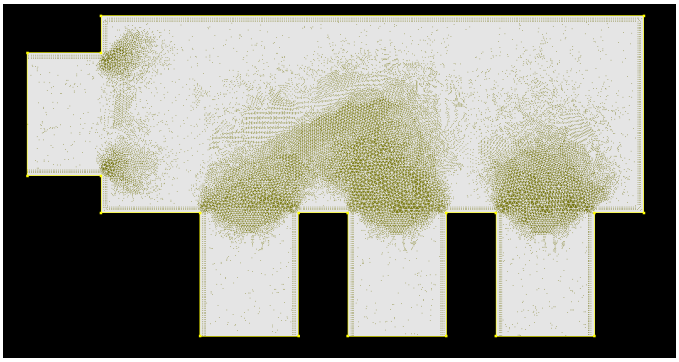

Figure 4. Final mesh chosen for study (roughly 234000 elements)

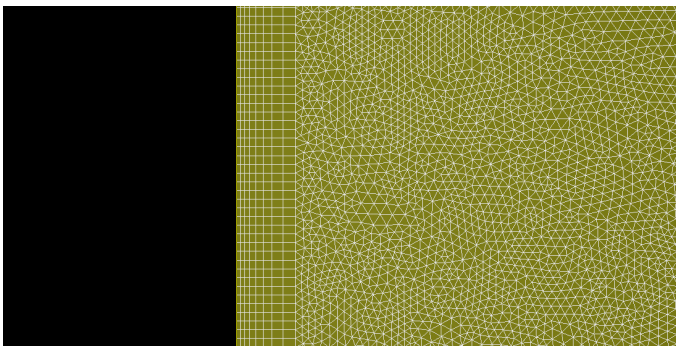

Figure 5. Detail of chosen mesh in near wall region

As shown above in Figure 5, boundary layers are visible in the near wall regions. A transition factor of 1.2 was used, which allowed for smooth development between the boundary layer and the unstructured grid region, ensuring more accurate results. These meshes all generated very respectable y-plus values, which is important parameter to determine cell sizes near wall domain and assess mesh quality.

RESULTS AND DISCUSSION

Laminar case

Simulations were firstly run at the laminar case. Unstructured meshes were designed ranging from 2k-100k elements and were run for laminar flow (0.1 m/s horizontal velocity) to conduct a mesh dependency study. Low mesh densities can present inaccurate solutions due to an incorrect definition of boundary layers. Fitting with the theoretical solution improves as mesh density increases, and finer meshes begin to converge to an identical solution. From this, it can be concluded that results have reached an asymptotic solution [15]. This can be observed in Figure 6 where results converge and can therefore be validated at 57.3k elements.

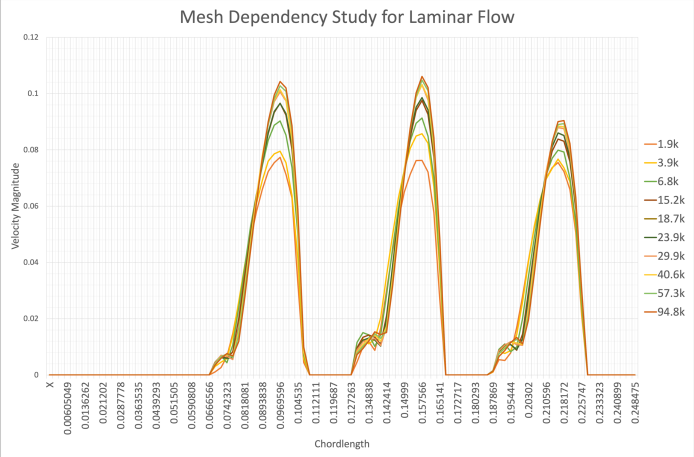

Figure 6 Mesh dependency study conducted for laminar flow

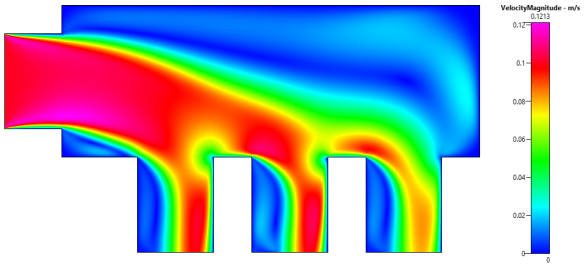

Figure 7 Flow analysis for laminar case

Figure 7 shows flow analysis in the laminar regime. Results are mapped through velocity magnitude parameters, identifying key areas where horizontal velocity is higher (pink and red regions, refer to legend above). As observable, flow starts at the inlet and disperses relatively evenly between the three outlets. Intake uniformity, and how it can be improved via designing new geometries, is discussed later in the report.

Turbulent flow

Intake manifolds exhibit air flow in the regulator chamber at extremely high velocities, with a Reynold's numbers above 3500. Thus, characterizing the flow as turbulent, which is the focal point of the investigation. A further mesh dependency study was conducted, this time making use of boundary layers in the unstructured meshes. High grid resolutions are required to represent passive scalar quantities close to the walls, and to accurately describe turbulent flows [16]. Hence, meshes designed in this case ranged from 30k to 480k elements.

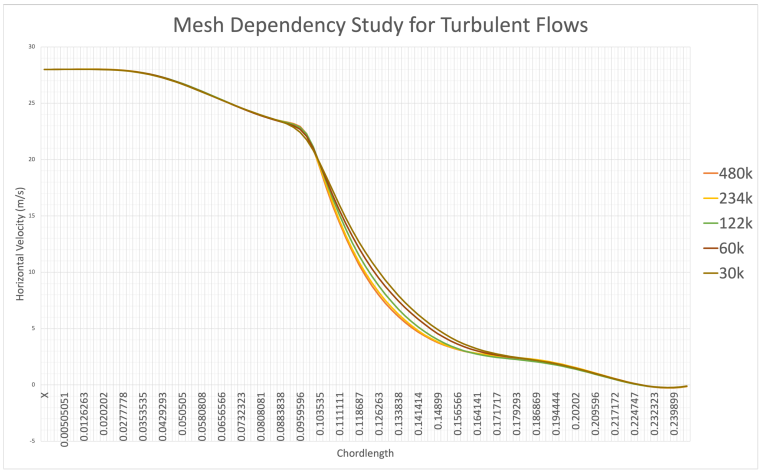

Figure 8 Mesh dependency study conducted for turbulent flows

As shown by Figure 8, convergence is only reached in finer meshes at turbulent flows. Horizontal velocity was plotted against chord length, with meshes doubling in number of elements. As the mesh size increases, the solution tended to converge closer to 240k elements. Upon closer inspection, one can notice that the 240k and 480k mesh almost overlap each other, demonstrating that further increasing mesh size won't impact the results. Grid independency is therefore achieved, legitimizing the proposed solution. To conduct the primary part of this investigation, the 234k mesh was chosen. On average, the 480k mesh took about 200 minutes to run, compared to 120 minutes for 234k. This reduction in run time further justifies the mesh choice, as more simulations can be run at a fraction of the time and computational power required. The Y-plus value is an important criterion for determining mesh quality in numerical simulations, hence it is an important parameter to consider before conducting simulations [17]. Y-plus is affected by kinematic viscosity and friction velocity, which are in turn affected by wall shear stress [7]. In laminar flow, the following variables are less relevant, meaning y-plus considerations are redundant. This explains why grid requirements differ between turbulent and laminar computations, as turbulent cases require higher grid resolutions in meshing, and therefore careful considerations of y-plus values.

For the 234k mesh and 480k mesh, y-plus was 12.93 (see Appendix I) and 11.13, respectively, when simulated at the highest velocities (28m/s). A y-plus of under 30 is deemed

acceptable in this application, meaning the small change between the two meshes can be considered negligible. As a final form of validation, relative error was computed. Between 234k-480k, the relative error was 1.6%, compared to a more significant error of 10.8% for 30k-480k mesh. Near zero errors, present at from 0.16 onwards on the x-axis of Figure 8 were disregarded as a measure of increasing accuracy.

CHANGE IN FLOW FEATURES AT HIGH REYNOLD'S NUMBERS

After the mesh was selected, simulations were run at various inlet velocities, ranging from 0.1m/s (laminar) – 28m/s (turbulent). Mass balance summaries, or mass flow rate at inlet and outlets was analyzed between all results, with an average value of 10E-6, signifying a small difference between inflow and outflow, which was deemed to be of acceptable accuracy for the scope of this study. Flow features were analyzed in the CFD+ VIEW post processing software using vector plots.

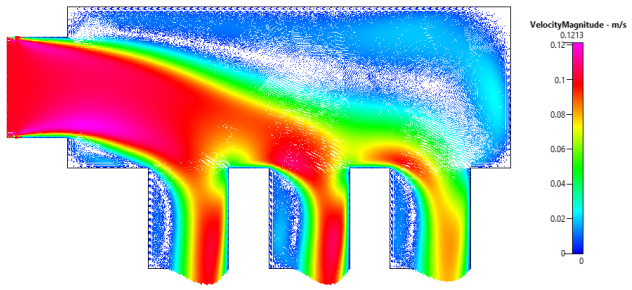

Figure 9 Vector flows in laminar case, 0.1 m/s

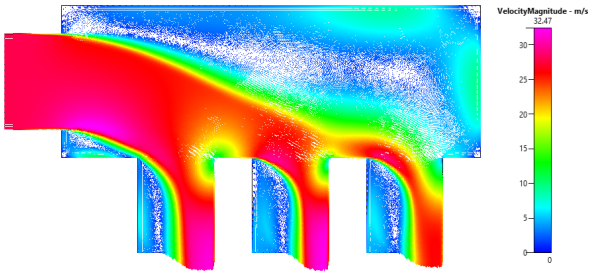

Figure 10 Vector flows at high turbulence, 28m/s

As evident in Figure 9 and 10, by increasing the horizontal velocity through the inlet and therefore incrementing Reynold's number, flow features tend to change. To begin, one can identify the production of vortices due to increased turbulence [18]. The most notable feature is that air flow via the inlet interacts with walls to form substantial vortex patterns [19]. By comparing the Figure 7 & 8 in the right most region of the regulator chamber, it can be observed that the vortices, are stronger and better defined in the turbulent case (higher Reynold's number), where larger velocities are present (refer to legend). Therefore, at higher Reynold's numbers, turbulent flow is more significant in the regulator cavity, forming backflows. This could lead to inefficiencies in the internal flow of the manifold, showing significant flaws in the base case geometry. As is discussed later, optimizing the geometry for this inlet manifold led to a better intake uniformity and internal flow, which will substantially impact the performance and efficiency in the engine.

HOW PRESSURE DROP AT INLET VARIES WITH REYNOLD'S NUMBER

The next aspect that investigated was how pressure drop at inlet varies with Reynold's number. Static pressure at the outlets was set to 0 in the simulation, meaning pressure drops could be measured by taking readings of pressure against chord length at the inlet. The chosen mesh was run at increasing flow velocities.

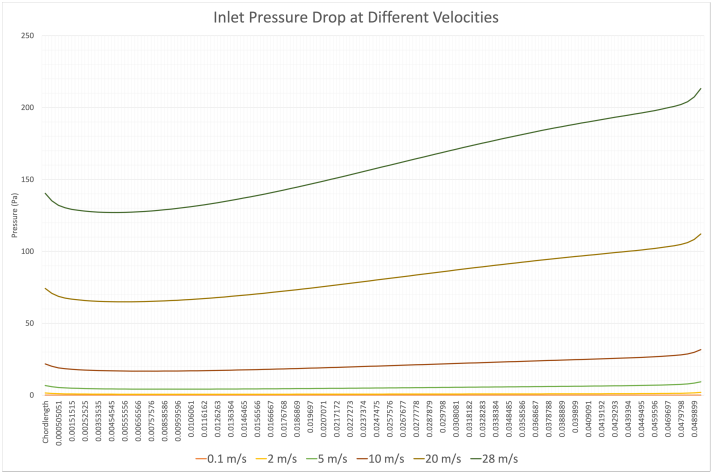

Figure 11 Pressure drop analysis for laminar and turbulent flows

Velocity (m/s)	Pressure Drop (Pa)	Percentage Change (%)
0.1	0.002955026	0
2	0.87651043	29562
5	5.3643906	181434
10	21.050691	712269
20	81.677768	2763929
28	159.79352	5407417

Figure 12 Average pressure drop at different velocities

Low pressure drop in an intake manifold is an essential factor in maximizing the mass of the pulled air into the cylinder [20]. As shown by Figure 11, increasing the Reynold's number, and therefore horizontal velocity, causes pressure drop to increase linearly. Between 28 and 20m/s the pressure doubles from 80 to 160Pa, whereas from 10 to 20m/s it quadruples, going from 20 to 80Pa. In the laminar case (0.1 m/s), pressure is almost negligible at 0.002 Pa. Figure 12 shows percentage change between all the velocities, relative

to the laminar case. From 0.1 to 2m/s, pressure increases almost 30,000%, whereas from 0.1 to 28 m/s it goes up by a staggering 5,400,000%. Pressure drops in the system, as well as wall shear stress tend to increase as phase velocity increases [21]. This is because as flow velocity increases, so do the friction forces of the air eroding against the interior walls of the system, resulting in higher pressure loss due to flow recirculation [22]. Thus, explaining why pressure drop increases with Reynold's number, and why turbulent flows lead to higher energy losses. The performance of the intake manifold can be therefore improved by making modifications in the regulator cavity, where recirculation is formed [23]. The identified linear relationship can also be explained through the Hagen-Poiseuille equation, which expresses the relationship between pressure, fluidic resistance, and flow rate. This implies that the fluid's velocity is directly proportional to the pressure drop at the inlets [24].

UPPER LIMIT FOR REYNOLD'S NUMBER IN CFD COMPUTATIONS

Intake manifold usually operate at high velocities of up to 167m/s, which is considered a turbulent flow. Thus, simulations could be run up to a Reynold's number of 571,758 for a realistic application of evaluating intake manifold performance in engines. Due to recent advancements in CFD software, running simulations at the following speeds is achievable, considering the flow analyzed is subsonic. However, issues will arise when the flow becomes supersonic. Supersonic flows originate through the generation of shock waves in which flow characteristics and streamlines vary in incoherent patterns [25]. This leads to distortions and deviations in the flow [26]. A supersonic flow can be measured by the Mach number. This can be described by the ratio of the velocity of an element travelling through a fluid to the speed of sound in that specific fluid [27]. When the Mach number is equal to 1, the flow can be considered supersonic. Thus, calculating for the speed of sound to be about 343 m/s, the maximum velocity that could be measured before a flow goes supersonic, and becomes insignificant in CFD computations, is 343 m/s. This would result in a Reynold's number of about 1174330.

EVALUATING INTAKE UNIFORMITY AT DIFFERENT VELOCITY CONFIGURATIONS

Intake flowrate uniformity is an important index to assess efficiency in an engine. It can be described by the homogeneity in dispersion of airflow through the three outlets. It is most desirable for an intake manifold to divide flow as evenly as possible between the three outlets. This was measured by plotting velocity against chord length at the three outlets, and average velocity was computed at each outlet. From this, mass flow rate was calculated by multiplying the average velocity by the density of air ($1.225 kg/m^3$) and the diameter of the outlets (0.04m). Uniformity in the intake manifold was analyzed by comparing mass flow rate at each outlet, as shown in Figure 13 below.

Velocity	Mass Flow Rate (kg/s)	Ratio
0.1 m/s	-0.00227	0.37
	-0.00200	0.33
	-0.00185	0.30
2m/s	-0.049653	0.41
	-0.03797	0.31
	-0.03468	0.28
5m/s	-0.12542	0.41
	-0.0947	0.31
	-0.08518	0.28
10m/s	-0.25058	0.41
	-0.18898	0.31
	-0.16996	0.28
20m/s	-0.50054	0.41
	-0.376970	0.31
	-0.33885	0.28
28 m/s	-0.70936	0.41
	-0.5327	0.31
	-0.385	0.28

Figure 13 Intake uniformity measured through average mass flow rate at each outlet

The intake uniformity in this configuration was spread quite unevenly, with majority of air flow occurring at the left most outlet, which is closest to the inlet, followed by the middle and rightmost outlet. The flow is split at a ratio of 0.41, 0.31 and 0.28, respectively for each outlet. It can be observed that the following distribution occurs at all turbulent velocities, suggesting that intake uniformity does not vary greatly by increasing velocity. There is however an exception for the laminar case, where the flow is dispersed at a ratio of 0.37, 0.33. and 0.30 for the left, middle and right outlet. This inconsistency might arise due to lower velocities allowing for more equal dispersion at the outlets, due to decreased pressure and vortex formations, as observed previously. The results obtained suggest that flow rate uniformity does not vary drastically with the increase of Reynold's numbers, similarly to the findings discussed by Alvarado et. Al, where flow uniformity was compared at different velocities and validated with two manifold configurations [28].

DESIGNING NEW GEOMETRIES

After having conducted investigations using the base case geometry, new inlet designs were configured as a measure of improving intake uniformity and therefore overall performance of the manifold.

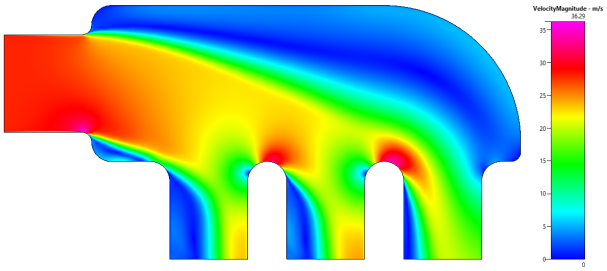

Figure 14 Alternative geometry 1

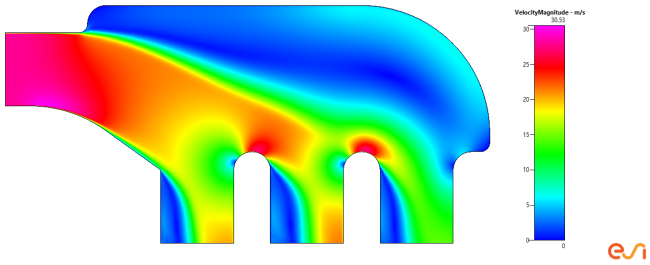

Figure 15 Alternative geometry 2

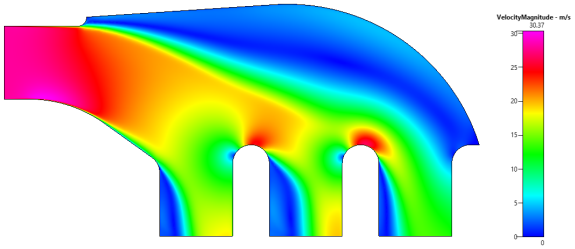

Figure 16 Finalized geometry

Figure 14-16 show the proposed solutions, configured using an iterative design approach, starting from the initial geometry, where each proposed concept is evolved from the previous design. The first modification executed was curving the right most section of the regulator chamber, where vortices and backflow occurred most often, as measure of redirecting the flow appropriately. As a result of this, a smaller volume was created combined with a decreased length of the regulatory chamber. According to the study conducted by Yabai et al., this lowers fluid loss along the manifold and improves uniformity [29]. The first iteration also featured rounded off dividing sectors between the outlets, in comparison to the straight edges provided in the base geometry. This is also called an elliptical bell mouth, deemed to be an effective feature that prevents any excessive flow separations, and provides smoother entry at the outlets [4].

The bell mouth implementation was made following a study conducted by Kumar et al., stating that introducing curved edges in the manifold provides many benefits such as a better directed flow and decreased resistance at the outlets [30].

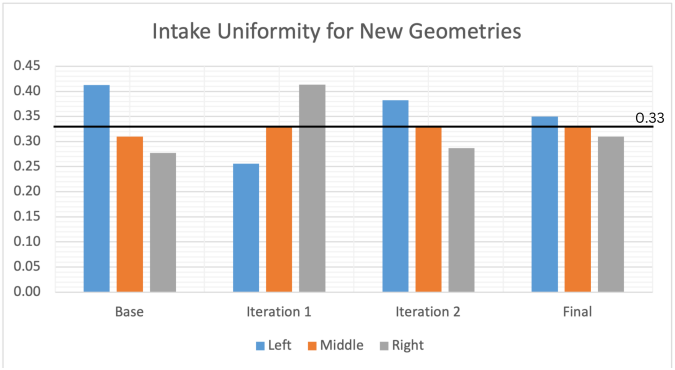

Figure 17 Intake uniformity described through ratios for different geometry configurations

Shown above is a comparison between the three proposed geometries, done by evaluating intake uniformity at each outlet through ratios as was previously executed in the study. Intake uniformity was chosen to be an acceptable parameter in investigating the quality of geometries as this is one of the most important aspects in assessing engine performance.

As observed in Fig. 17, the first iteration did not prove successful and exhibited a similar intake uniformity compared to the base case but flipped around (right most outlet had highest flow rate). Other factors that affect intake uniformity were investigated, including inlet direction, inlet diameter, and the length of the manifold outlets [3]. Thus, in the next geometry, the inlet diameter was reduced from 50mm to 40mm, as a means of increasing horizontal velocity. This was done by interpreting the mass flow rate equation, where one can infer that velocity is directly proportional to the length. A problem encountered in the previous geometry was the left outlet had much lower air flow, so in the new configuration the inlet direction was changed to be more directed the left outlet. This yielded much better results, with a ratio of 0.38, 0.33, 0.29, respectively for the left, middle and right outlet. The final changes, as shown in Figure 14, included tweaks in the angle and direction of the inlet, as well as further reductions in the volume and a more pronounced curvature which was designed to compensate for the vortices examined in the first part of this study. The direction of flow was also examined and considered for this last iteration. The third and final geometry was undoubtedly the best performing, with an almost even intake uniformity of 0.35, 0.33, 0.31, respectively at the three outlets. While this latest evolution exhibits much more promising results

compared to the base geometry, it could be tweaked further, through incremental changes in the inlet direction angle and regulator chamber volume and shape. This could prove highly beneficial, as improving intake uniformity slightly could radically improve performance in an engine.

HYPOTHESIS AND LIMITATIONS

Hypothesis:

- Heat transfer was assumed to be negligible in the following investigation, with a constant temperature of 300K used to conduct simulations. However, in real life applications manifolds are installed close to the engine which makes the solution provided less accurate
- Pressure at the outlet was assumed to be static, which is incoherent from what would occur in real life scenario
- Air density varies at different temperatures. Despite this, a constant density of 1.225kg/m^3 was used, which likely skewed results

Limitations:

- K-ε turbulence model has shortcomings such as simulating near wall flows (must implement wall functions), predicting k values etc. [31]
- The mesh generation software (CFD Geom) has some limitations, such as inability to preview meshes, predicting number of elements and refining at local points
- The geometry was constructed in 2D, which is limiting as inlet manifolds are 3D configurations, so a 3D model would have allowed for a more accurate simulation

CONCLUSIONS

The following study focused on investigating flow features in a complex manifold configuration, and ultimately redesigning the geometry to improve its efficiency. The intake manifold was investigated at its core, including how it functions, it's relevant applications in the automotive industry as well as the most relevant geometric aspects to consider in the fabrication process that ultimately impact engine performance. At first, a base 2D geometry was provided to conduct simulations. The simulations were run at increasing Reynold's numbers, at respective velocities of 0.1, 2, 5, 10, 20 and 28m/s, describing laminar and turbulent flows. For the laminar case, unstructured meshes were used ranging for 2k-100k elements, without the use of boundary layers as flow in near wall regions does not impact results greatly. A mesh dependency study was conducted for laminar and turbulent case, where grid independence was reached at 57k and 234k elements, respectively. Thus, meaning mesh size did not impact the accuracy of results. The chosen mesh consisted of 234k elements, using boundary layers to allow for accurate grid resolution close to the walls, which is important when operating with the k-ε turbulence model, which was used for majority of simulations. Y-plus values were examined, ranging from 10-30 according to the mesh sizes (24k-480k). The chosen mesh used to run simulations exhibited a y-plus of 12.93 (see appendix), which is adequate value for the scope of this study. Flow features were analyzed between increasing Reynold's number, mainly for laminar (0.1m/s) and turbulent flow (28m/s) using vector plots. For the most part, these remained unchanged, with vortices created in the right section of the regulator chamber. However, backflows were much more defined at higher velocities due to increased turbulences near the manifold bend (see Figure 7 and 8). Pressure drops at the inlets were analyzed at increasing Reynold's number, with a linear relationship identified between pressure and flow velocity, which is in accordance with Hagen-Poiseuille's equation. The upper limit of Reynold's number for these computations was also explored by examining when the flow goes from subsonic to supersonic, which was identified to be at velocities of 343 m/s or above and a Reynold's number of 1174330, using Mach's number threshold of 1.

Intake uniformity was evaluated by evaluating mass flow rate at each outlet and compared at different velocities. These values stayed the same, for turbulent flows, with a ratio of 0.41, 0.31 and 0.28, for the left, middle and right outlets, and slightly varied at laminar with 0.37, 0.33 and 0.30, respectively. Lastly, new geometries were constructed, iterating through 3 configurations. Main modifications included, curving the right section of the regulator chamber, decreasing the regulator cavity volume, reducing the diameter of the inlet to increase flow velocity, introducing elliptical bell-mouths at the outlets, and varying inlet direction to direct flow into desired outlets. The last proposed geometry exhibited an intake uniformity of 0.35, 0.33, 0.31, an enormous improvement compared to the base geometry. Continuing to evolve this geometry, by increasing the intake uniformity could present great opportunities in developing the efficiency of the intake manifold, and therefore the overall engine performance.

APPENDIX

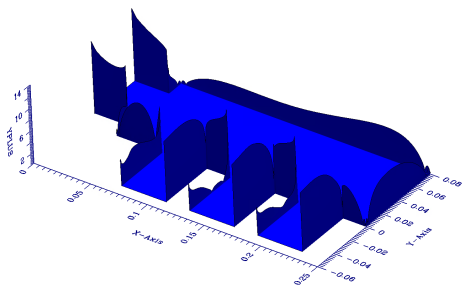

Appendix I – y plus carpet plot for chosen mesh of 234k elements

REFERENCES

[1] "What is an Intake Manifold Gasket | Fel-Pro Gaskets." https://www.felpro.com/gaskets-101/all-about-intake-manifold-gaskets.html (accessed Nov. 15, 2022).

[2] "Beginner's Guide: What Is an Intake Manifold (and What Does It Do)? | Haynes Manuals." https://haynes.com/en-us/tips-tutorials/what-is-car-inlet-intake-manifold (accessed Nov. 15, 2022).

[3] N. S. M Goncalves *et al.*, "Flow analysis of engine intake manifold based on computational fluid dynamics," *J Phys Conf Ser*, vol. 916, no. 1, p. 012043, Oct. 2017, doi: 10.1088/1742-6596/916/1/012043.

[4] S. Seshadri, "DESIGN AND CFD ANALYSIS OF THE INTAKE MANIFOLD FOR THE HONDA CBR250RR ENGINE," 2015.

[5] "Meshing in FEA: Structured vs Unstructured meshes | OnScale." https://onscale.com/blog/meshing-in-fea-structured-vs-unstructured-meshes/ (accessed Nov. 15, 2022).

[6] H. K. Versteeg and W. Malalasekera, *An Introduction to Computational Fluid Dynamics - THE FINITE VOLUME METHOD*, Second Edition. Essex: Pearson Education Limited , 2007.

[7] "What is y+ (yplus)? - Using SimScale / Fluid Flow / CFD - SimScale CAE Forum." https://www.simscale.com/forum/t/what-is-y-yplus/82394 (accessed Nov. 14, 2022).

[8] J. D. Jr. Anderson, *Computational Fluid Dynamics - The Basics With Appications*. New York : McGraw-Hill, Inc. , 1995.

[9] "What is Turbulent Flow? Computational Fluid Dynamics | SimScale." https://www.simscale.com/docs/simwiki/cfd-computational-fluid-dynamics/what-is-turbulent-flow/ (accessed Nov. 15, 2022).

[10] ESI Group, *CFD-ACE+ USER GUIDE*. Paris: ESI Group, 2020.

[11] "How to Choose the Right Intake for Your Engine, Part 1." https://www.motortrend.com/how-to/1602-how-to-choose-the-right-intake-for-your-engine-part-1/ (accessed Nov. 15, 2022).

[12] E. Shashi Menon, "Fluid Flow in Pipes," *Transmission Pipeline Calculations and Simulations Manual*, pp. 149–234, 2015, doi: 10.1016/B978-1-85617-830-3.00005-5.

[13] "Laminar and Turbulent Flow | Engineering Library." https://engineeringlibrary.org/reference/laminar-and-turbulent-fluid-flow-doe-handbook (accessed Nov. 15, 2022).

[14] K. C. Chitale, O. Sahni, S. Tendulkar, R. Nastasia, M. S. Shephard, and K. E. Jansen, "Boundary layer adaptivity for transonic turbulent flows," *21st AIAA Computational Fluid Dynamics Conference*, 2013, doi: 10.2514/6.2013-2445.

[15] A. Guardo, M. Coussirat, F. Recasens, M. A. Larrayoz, and X. Escaler, "CFD study on particle-to-fluid heat transfer in fixed bed reactors: Convective heat transfer at low and high pressure," *Chem Eng Sci*, vol. 61, no. 13, pp. 4341–4353, Jul. 2006, doi: 10.1016/J.CES.2006.02.011.

[16] A. Sakowitz, M. Mihaescu, and L. Fuchs, "Turbulent flow mechanisms in mixing T-junctions by Large Eddy Simulations," *Int J Heat Fluid Flow*, vol. 45, no. 1, pp. 135–146, Feb. 2014, doi: 10.1016/J.IJHEATFLUIDFLOW.2013.06.014.

[17] X. Liu, Q. Yuan, M. Zhao, W. Cui, and · Tong Ge, "Multiple objective multidisciplinary design optimization of heavier-than-water underwater vehicle using CFD and approximation model," *J Mar Sci Technol*, vol. 22, doi: 10.1007/s00773-016-0399-5.

[18] A. C. Chandekar and B. K. Debnath, "Effect of intake manifold design on the mixing of air and bio-CNG in a port-injected dual fuel diesel engine," *J Therm Anal Calorim*, vol. 141, no. 6, pp. 2295–2309, Sep. 2020, doi: 10.1007/S10973-020-09591-1/TABLES/3.

[19] M. A. Jemni, G. Kantchev, and M. S. Abid, "Influence of intake manifold design on in-cylinder flow and engine performances in a bus diesel engine converted to LPG gas fuelled, using CFD analyses and experimental investigations," *Energy*, vol. 36, no. 5, pp. 2701–2715, May 2011, doi: 10.1016/J.ENERGY.2011.02.011.

[20] K. Gocmen and H. S. Soyhan, "An intake manifold geometry for enhancement of pressure drop in a diesel engine," *Fuel*, vol. 261, p. 116193, Feb. 2020, doi: 10.1016/J.FUEL.2019.116193.

[21] M. Ballesteros Martínez, E. Pereyra, and N. Ratkovich, "CFD study and experimental validation of low liquid-loading flow assurance in oil and gas transport: studying the effect of fluid properties and operating conditions on flow variables," *Heliyon*, vol. 6, no. 12, p. e05705, Dec. 2020, doi: 10.1016/J.HELIYON.2020.E05705.

[22] K. Srivallika, K. Swathi, B. V. Lakshmi, D. H. Bhanu, B. Harini, and T. R. Devi, "Cost Efficient Designing of Quantum Cellular Automata Based Code Converters," *Int J Sci Res Sci Technol*, vol. 9, no. 3, pp. 667–674, Jun. 2022, doi: 10.32628/IJSRST2293133.

[23] R. Thamaraikanan, M. Anish, B. Kanimozhi, T. George, and V. George Koshy, "Design and Analysis of an Intake Manifold in an IC Engine," *Applied Mechanics and Materials*, vol. 766–767, pp. 1021–1027, Jun. 2015, doi: 10.4028/WWW.SCIENTIFIC.NET/AMM.766-767.1021.

[24] M. Nauenberg, "A paradox with the Hagen-Poiseuille relation for viscous fluid flow," *Am J Phys*, vol. 82, no. 1, p. 82, Dec. 2013, doi: 10.1119/1.4825138.

[25] V. B. Baranov, "Possible effects of the interstellar magnetic field on the heliospheric structure and H-atom penetration to the solar system," *COSPAR Colloquia Series*, vol. 11, no. C, pp. 99–108, 2001, doi: 10.1016/S0964-2749(01)80020-2.

[26] H. S. Tsien, "Problems in Motion of Compressible Fluids and Reaction Propulsion," *Collected Works of Hsue-Shen Tsien (1938-1956)*, pp. 21–75, 2012, doi: 10.1016/B978-0-12-398277-3.50003-8.

[27] "Flow Regimes – The Physics Hypertextbook." https://physics.info/turbulence/ (accessed Nov. 14, 2022).

[28] B. Ramos-Alvarado, P. Li, H. Liu, and A. Hernandez-Guerrero, "CFD study of liquid-cooled heat sinks with microchannel flow field configurations for electronics, fuel cells, and concentrated solar cells," *Appl Therm Eng*, vol. 31, no. 14–15, pp. 2494–2507, Oct. 2011, doi: 10.1016/J.APPLTHERMALENG.2011.04.015.

[29] Y. Yabai, chen and L. Chunying, "The Optimization Analysis of Diesel Engine Intake Manifold based on UG and FLUENT," *International Journal of Research in Engineering and Science (IJRES) ISSN*, vol. 4, pp. 40–46, 2016, Accessed: Nov. 14, 2022. [Online]. Available: www.ijres.org40|

[30] R. Ramesh Kumar *et al.*, "Vibration analysis of composite exhaust manifold for diesel engine using CFD," *Case Studies in Thermal Engineering*, vol. 32, p. 101853, Apr. 2022, doi: 10.1016/J.CSITE.2022.101853.

[31] P. S. Bernard, "Limitations of the near-wall k-epsilon turbulence model," *https://doi.org/10.2514/3.9316*, vol. 24, no. 4, pp. 619–622, May 2012, doi: 10.2514/3.9316.

[32] Ventikos, Y. 2022.Computational Fluid Dynamics Modelling Turbulent Flows: Turbulence Models. MECH0059. Advanced Computer Applications in Engineering. 31/10/2022, University College London.